ELSEVIER

Earth and Planetary Science Letters 194 (2002) 327–341

EPSL

www.elsevier.com/locate/epsl

Relative geomagnetic paleointensity from the Jaramillo Subchron to the Matuyama/Brunhes boundary as recorded in a Mediterranean piston core

Jaume Dinarès-Turell [a,*], Leonardo Sagnotti [a], Andrew P. Roberts [b]

[a] *Istituto Nazionale di Geofisica e Vulcanologia, Via di Vigna Murata 605, 00143 Rome, Italy*
[b] *School of Ocean and Earth Science, University of Southampton, Southampton Oceanography Centre, European Way, Southampton SO14 3ZH, UK*

Received 12 July 2001; received in revised form 18 October 2001; accepted 18 October 2001

Abstract

Piston core LC07, located west of the Sicily Strait in the Mediterranean Sea, unambiguously records the Matuyama/Brunhes (M/B) and the upper Jaramillo polarity reversals, with similar average sediment accumulation rates (SARs) for the Brunhes Chron (2.29 cm/kyr) and late Matuyama Chron C1r.1r (2.19 cm/kyr). We report a relative paleointensity record for the interval spanning the M/B boundary down into the Jaramillo Subchron, which is unique in the Mediterranean because existing records from this basin cover only the last 80 kyr. The average SAR in core LC07 is used to translate the depth-related paleointensity record to the time domain; the ratio of anhysteretic remanent magnetization to low-field magnetic susceptibility is climatically sensitive and is used to tune the age model. This correlation produces a good fit to the global ice volume model derived for summer insolation at 65°N. With this age model, a paleointensity minimum in association with the M/B boundary has a duration of about 4–5 kyr, while the directional change has a duration of <3 kyr. A second paleointensity minimum of similar duration is found about 16 kyr below the M/B boundary. This feature (precursor or 'dip' in the literature) has previously been recognized at the same time interval in many marine records, which reinforces the validity of our age model. Other relative paleointensity minima are found within chron C1r.1r, and, within the uncertainties of the respective age models, these minima coincide with those observed from the few published coeval paleointensity records. In particular, there is good correspondence between the ages of minima at about 0.92 and 0.89 Ma, which probably correlate with two geomagnetic excursions (Santa Rosa and Kamikatsura, respectively) that have been recorded in lava flows and dated using the $^{40}Ar/^{39}Ar$ technique. In contrast, a recently dated excursion at 0.83 Ma from La Palma seems to correspond to a paleointensity maximum. This observation is opposite to that expected and this excursion needs to be confirmed. In contrast to some recently published paleointensity records, spectral analysis of the LC07 record does not reveal identification of significant power at the orbital obliquity frequency.

Keywords: paleointensity; magnetic field; Matuyama Chron; Jaramillo Subchron; Brunhes Chron; Mediterranean Sea

1. Introduction

The possibility of retrieving relative intensity variations of the Earth's magnetic field from sedi-

* Corresponding author. Fax: +39-6-5186 0397.
E-mail address: dinares@ingv.it (J. Dinarès-Turell).

0012-821X/02/$ – see front matter
PII: S0012-821X(01)00563-5

ments [1] and the availability of long marine records recovered by drilling deep-sea sediments allow the documentation of continuous geomagnetic paleointensity variations back in time, in contrast to volcanic rocks which represent spot readings of the field. Documenting long-term variations in the dipole field during periods of stable polarity and field evolution across reversals or other geomagnetic features (i.e., excursions, tiny wiggles) is critical to understanding the geodynamo. Furthermore, the relationship between geomagnetic proxies and the Earth's climatic system and external climatic forcing needs to be assessed [2,3]. The wealth of suitable sedimentary sequences spanning the youngest part of the geological record allowed the compilation of a global geomagnetic paleointensity stack, Sint-200 [4]. More recently, as sufficient records have became available for the entire Brunhes normal polarity chron (0–778 ka), a new extended stack, Sint-800, has been compiled [5]. Consequently, there is growing interest in retrieving sedimentary paleointensity proxies throughout the Matuyama Chron and beyond in order to understand longer-term geomagnetic evolution. A first long sedimentary record of relative paleointensity spanning the last 4 million years from the equatorial Pacific Ocean was provided by Valet and Meynadier [6]. The long-term saw-tooth behavior observed by Valet and Meynadier [6] has been claimed to be a consequence of unremoved viscous magnetizations, although the finer-scale features remain valid as indicated by thermally derived paleointensity proxies [7]. A paleointensity stack for the Ontong–Java Plateau (western equatorial Pacific Ocean) (0.778–2.852 Ma) has also been derived using the thermal approach [8].

Technical advances of long-core magnetometers and routine continuous (u-channel) sampling and measurement of marine cores favors the development of relative paleointensity records. A drawback in many recovered marine cores is the fact that they are frequently affected by severe coring-related magnetic overprints that often render them unsuitable for paleomagnetic purposes [9,10]. In addition, diagenetic dissolution of magnetic minerals in organic-rich sediments is known to occur, which hampers the acquisition of high-resolution field records [11–13]. Most Mediterranean cores collected by the Ocean Drilling Program and others have been affected by strong secondary magnetic overprints, magnetite dissolution and/or other diagenetic artifacts [13–15]. This has limited attempts to develop longer Mediterranean paleointensity records.

We present paleomagnetic and rock magnetic data measured on u-channels from a piston core located near the Strait of Sicily that proved to be suitable for relative paleointensity determinations. The aim of this study is to document the first relative paleointensity data from the Mediterranean basin spanning the interval across the Matuyama/Brunhes (M/B) boundary through to the Jaramillo Subchron. We have focused on this time interval because is relatively poorly described compared to the Brunhes Chron (see [5]).

2. Material and methods

Mediterranean piston core LC07 (length 23.66 m, latitude/longitude 38°08.72′N/10°04.73′E, water depth 488 m) was collected by the R.V. *Marion Dufresne* in 1995 (MAST II PALAEOFLUX Program) from a location north of the Skerki channel at the western side of the Sicily Strait (Fig. 1). Core LC07 was continuously sampled with ca. 1 m long u-channel samples [16] at the BOSCOR repository at the Southampton Oceanography Centre, UK. The sediment throughout the interval studied here is a visually homogeneous gray to olive gray foraminiferal nannofossil ooze. The upper 0.5 m of the core was unsuitable for u-channel sampling due to sediment disturbances. Magnetic measurements on the u-channels were made using a 2G Enterprises high-resolution (45 mm diameter) pass-through cryogenic magnetometer at the Istituto Nazionale di Geofisica e Vulcanologia in Rome, Italy. Measurements on the u-channels were made at 1 cm spacing, although smoothing occurs due to the half-powder width of the response function of the magnetometer pick-up coils [17] (4.8 cm for the radial x and y directions and 5.9 cm for the axial z direction in the Rome system). The data from the upper and lower 4 cm of each u-channel

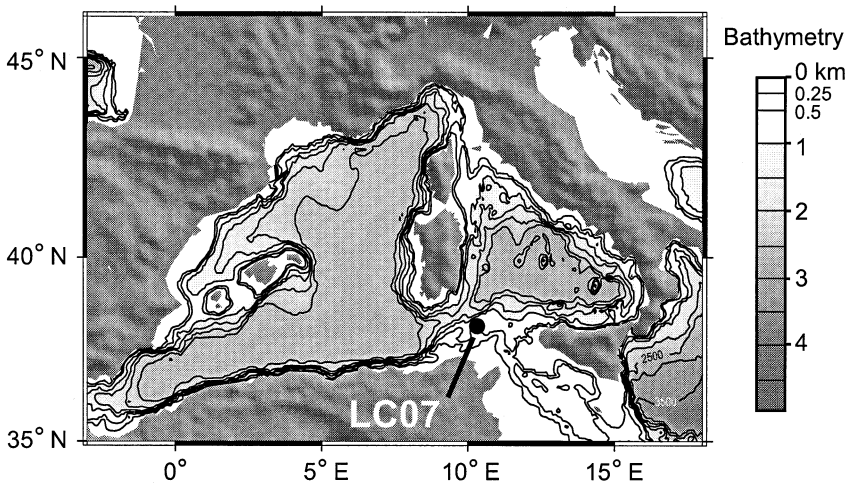

Fig. 1. Map of the Mediterranean Sea with location and setting of core LC07 in the western Mediterranean Sea.

were not used because these data are affected by edge effects due to the width of the magnetometer response function. Volume magnetic susceptibility (κ) was measured on the u-channels using an in-line 45 mm diameter loop (MS-2C, Bartington Instruments). The natural remanent magnetization (NRM) was measured and progressively demagnetized using stepwise peak alternating fields (AF) of 10, 20, 30, 40, 50, 60, 80 and 100 mT. An anhysteretic remanent magnetization (ARM) was imparted using a 100 mT peak AF with a 0.1 mT direct current (DC) bias field. The ARM was measured and demagnetized at the same peak AFs used for NRM demagnetization. Isothermal remanent magnetizations (IRMs) were imparted to the z axis of the u-channels in a steady DC field of 0.9 T. The IRMs were measured before demagnetization and then after demagnetization at 10, 20, 30, 40, and 60 mT. Finally, the remanence obtained by first imparting a new IRM at 0.9 T, followed by a back-field IRM at 0.3 T, was measured. and used to calculate the S-ratio ($= -\mathrm{IRM}_{-0.3\mathrm{T}}/\mathrm{IRM}_{0.9\mathrm{T}}$).

3. Results

3.1. Magnetostratigraphy

Orthogonal projections of NRM demagnetization data indicate that a characteristic remanent magnetization (ChRM) is isolated after removal of a low-coercivity viscous secondary component at about 10–20 mT (Fig. 2c), with less than 2% of the initial remanence remaining at 100 mT. The ChRM component was calculated at 1 cm intervals down-core by the least-squares line-fitting procedure [18]. The interval from 30 mT to 80 mT (five steps) was chosen for ChRM calculations. The computed ChRM inclinations and the maximum angular deviation (MAD) values are plotted against depth in Fig. 2a. MAD values are generally lower than 3°, which indicate well-defined ChRM components along the entire core. Occasionally, higher MAD angles ($< 18°$) are observed, some of which are related to magnetic reversals or paleointensity minima (see below). The inclination values for core LC07 are compatible with the expected geomagnetic axial dipole (GAD) inclination for the site latitude (Fig. 2b). The down-core ChRM inclination values indicate that core LC07 contains the entire Brunhes (C1n) and the upper part of the Matuyama chrons (C1r.1r and part of C1r.1n or the Jaramillo Subchron). The location of the M/B and upper Jaramillo (UJ) reversals at 17.83 mbsf and 22.48 mbsf, respectively, indicates that the mean sediment accumulation rate (SAR) is 2.29 cm/kyr for the Brunhes Chron and 2.19 cm/kyr for chron C1r.1r. Extrapolating the latter SAR down-core

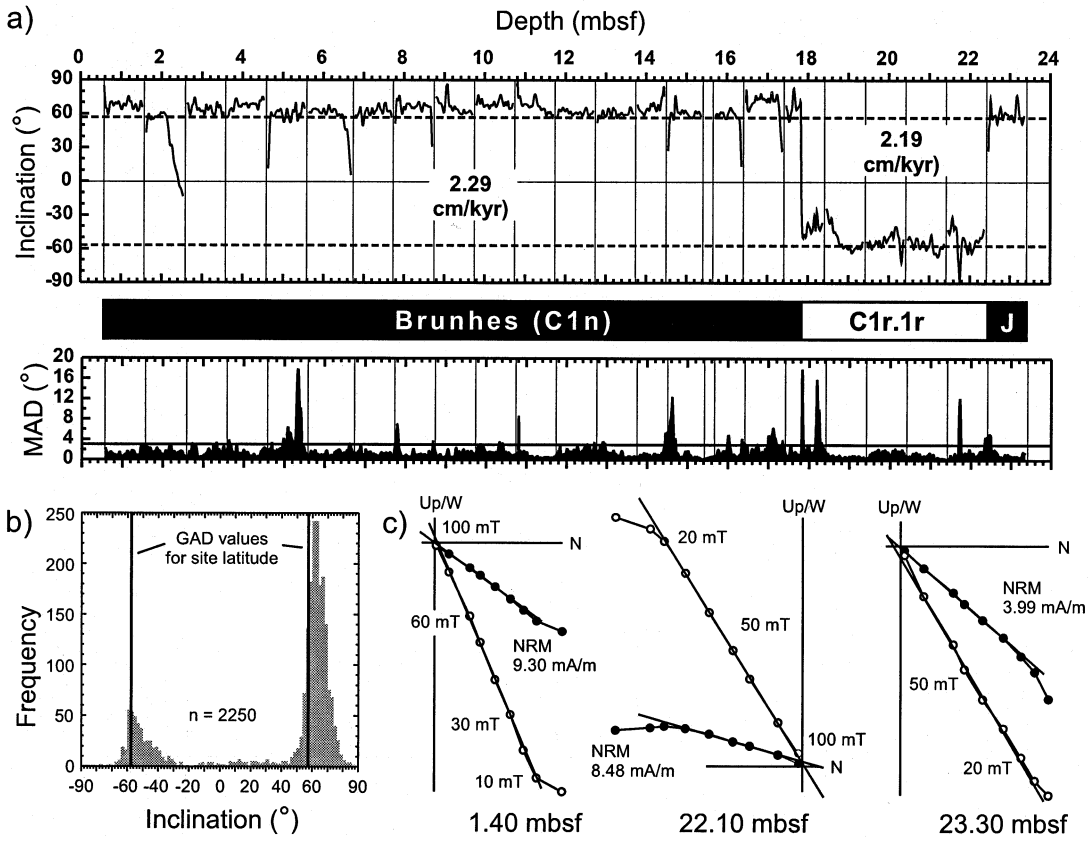

Fig. 2. (a) Inclination and maximum angular deviation (MAD) of the ChRM component computed from the 30–80 mT demagnetization steps. The magnetostratigraphic interpretation and the mean sediment accumulation rates (SARs) for different chrons are shown. (b) Histogram of normal- and reversed-polarity ChRM inclinations. The vertical lines indicate inclinations for a geocentric axial dipole (GAD) field at the site latitude. (c) Representative examples of normal and reversed polarity orthogonal vector component diagrams at different depths.

gives an age estimate of 1.031 Ma for the base of the core (i.e., core LC07 reaches 48% into the Jaramillo Subchron). The astronomically calibrated ages of 0.778 Ma (M/B) and 0.990 Ma (UJ) are used for these reversal boundaries [19,20].

3.2. The M/B reversal

The M/B reversal occurs within a single u-channel. Core LC07 was not azimuthally oriented but paleomagnetic declinations for this u-channel are coincidentally close to the S and N direction before and after the reversal, respectively. The declination, inclination, MAD of the ChRMs and the NRM at different demagnetization steps along this u-channel are plotted in Fig. 3a. The NRM intensities normalized by ARM, both after demagnetization at 20 mT, are also shown in Fig. 3a. The normalized NRM intensity is considered an indicator for geomagnetic relative paleointensity, as discussed below. In Fig. 3b, examples of orthogonal demagnetization plots from above, within, and below the M/B reversal are shown. There appears to be an interval of about 5 cm thickness, with 'intermediate' directions in the declination and inclination plots (Fig. 3a). The demagnetization trajectories for NRM measurements at 17.80, 17.82, and 17.84 m (Fig. 3b) illustrate the transition. A fully normal-polarity

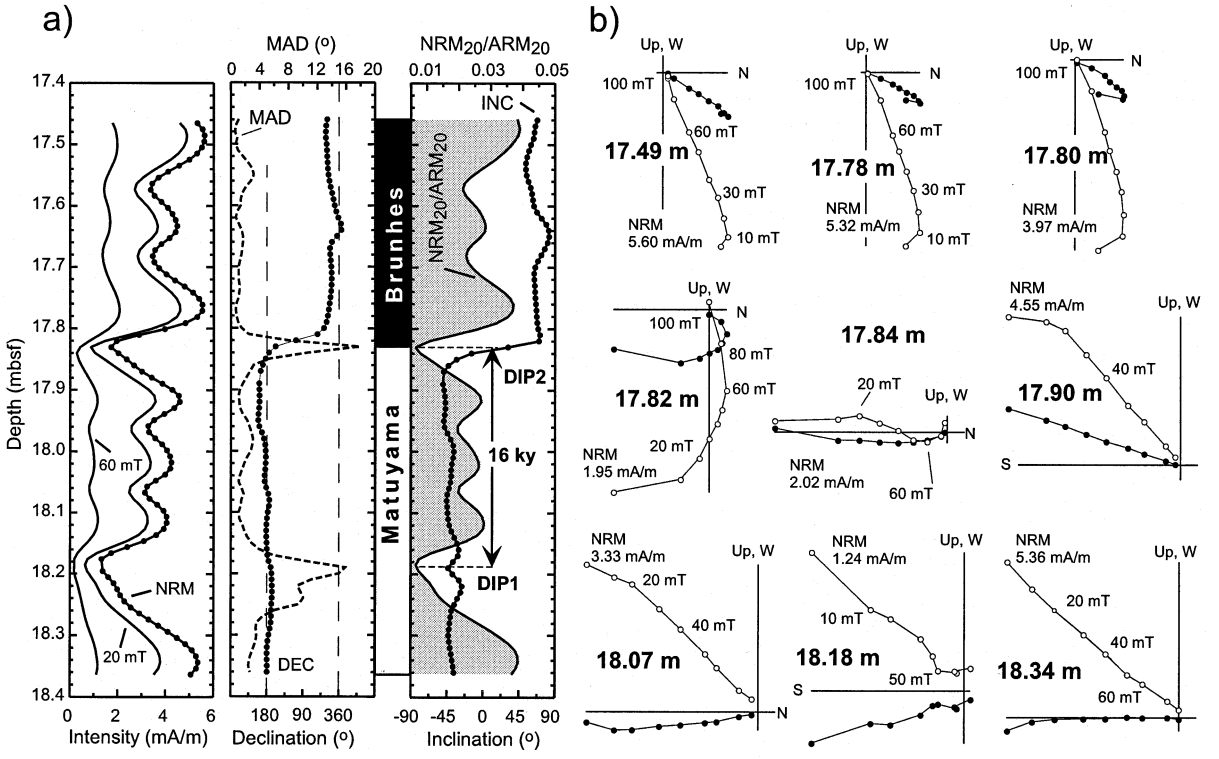

Fig. 3. (a) NRM intensity (prior to demagnetization and after AF demagnetization at 20 mT and 60 mT), declination, inclination and MAD along the u-channel containing the M/B reversal. The NRM intensity normalized by the ARM is shown as a shaded curve where two relative minima are labeled DIP1 and DIP2, respectively (see text for explanation). (b) Orthogonal vector component diagrams illustrating the M/B polarity transition.

ChRM component is observed at 17.80 m. A swing toward northerly declinations and positive inclinations at 17.82 m is seen, and finally a shallow reversed-polarity direction at 17.84 is observed although it is not yet fully reversed and linear as depicted for data at 17.90 m. Note that computing a ChRM from 30 to 80 mT for data at 17.82 and 17.84 m produces an 'intermediate' direction with high MAD angles, as shown in Fig. 3a. Given that the u-channel data are smoothed and that measurements are only independent at 4–5 cm intervals, it can be speculated that the M/B reversal probably occurs across a stratigraphic interval of just 2 or 3 cm at the most in core LC07. Using an average SAR of 2.24 cm/kyr, as derived from mean SAR values in the Brunhes and C1r.1r chrons, the duration of the M/B directional transition was <3 kyr. The NRM/ARM has a minimum or 'dip' coinciding with the M/B reversal at 17.83 mbsf and is labeled DIP2 in Fig. 3a, following the nomenclature of Kent and Schneider [21]. Another minimum in relative paleointensity (DIP1 in Fig. 3a) is observed $\sim$36 cm below DIP2. The intensity of this pre-reversal minimum is comparable in magnitude to that of the reversal. No directional excursion is observed associated with DIP1 (only a local increase in the MAD value is observed which denotes reduced NRM integrity; Fig. 3). DIP1 in core LC07 occurs $\sim$16 kyr before the M/B reversal (assuming a mean SAR of 2.24 cm/kyr) and is therefore consistent with the age of DIP2 from many other sedimentary paleointensity records [21,22]. The presence of this global feature supports the reliability of the NRM/ARM ratio as a paleointensity proxy in core LC07 and indicates that the mean SAR, as constrained by magnetostratigraphy, provides a consistent age estimate.

3.3. Rock magnetic properties and age model

Low-field magnetic susceptibility κ, and the IRM, ARM and NRM intensities generally reflect variations in the concentration of ferrimagnetic minerals. However, κ and IRM are biased toward coarser-grained ferrimagnetic particles and ARM and NRM are more strongly affected by fine-grained particles. The NRM intensity also partly reflects the intensity of the geomagnetic field at the time of magnetization lock-in. For magnetic assemblages dominated by magnetite, the ratio ARM/κ is indicative of magnetite grain sizes within the fraction from stable single-domain through to multidomain sizes [23]. For core LC07, dominance of magnetite is compatible with the AF demagnetization characteristics of the NRM illustrated in Fig. 2c. This conclusion is confirmed by electron diffraction analysis during scanning electron microscope observations of magnetic extracts. However, a relatively small high-coercivity (goethite/hematite) contribution is also likely. This is shown by *S*-ratios that usually range from 0.90 to 0.98 (Fig. 4). The down-core variation of the concentration-dependent parameters IRM and ARM for the examined part of core LC07 (Fig. 4) do not exceed a factor of 2, when a thin interval with relatively low remanence values at about 21.7 mbsf is excluded. The *S*-ratio for this interval is 0.90 (Fig. 4), which indicates a relatively increased contribution of the high-coercivity fraction. Down-core variations of ARM_{20mT}/κ (Fig. 4) show various maxima and minima, which are indicative of grain size variations (i.e., larger values indicate smaller grain sizes). The median destructive field of ARM (MDF_{ARM}) varies from 33 mT to 40 mT and generally follows the ARM_{20mT}/κ trend. Use of a 100 mT AF to impart an ARM means that high-coercivity particles will not significantly contribute to the ARM. Thus, good agreement between MDF_{ARM} and ARM_{20mT}/κ variations (Fig. 4) supports the use of ARM_{20mT}/κ as a grain size proxy in this case.

A detailed and reliable age model is necessary for the analysis and comparison of paleointensity data from different cores. An oxygen isotope stratigraphy, which is the most widely used chronostratigraphic dating tool for marine sediments of the Brunhes Chron, is not yet available for core LC07. However, several studies have demonstrated the usefulness of rock magnetic parameters as climatic proxies in marine sediments and have used them to establish age models for cores where independent dating was not available by correlating a rock magnetic parameter to an appropriate climatic target curve (i.e., reference oxygen isotopic curve or astronomical solutions) [24,25]. Here, we examine the lower part of the LC07 record where the presence of magnetostratigraphic boundaries (i.e., the M/B and UJ reversals) provide tie points to constrain the age model.

The M/B reversal is established to have occurred at 778 kyr, within interglacial marine isotopic stage (MIS) 19 [19]. The M/B boundary in core LC07 occurs at 17.83 mbsf, within a prominent ARM_{20mT}/κ maximum (Fig. 4), which can be inferred to correlate with MIS 19. Down-core variations of ARM_{20mT}/κ (and also MDF_{ARM}) (Fig. 4) can easily be correlated to an oxygen isotopic curve (we used the benthic record from ODP Site 677 [20] as the target curve and the AnalySeries software [26] for correlation purposes). Different ARM_{20mT}/κ maxima and minima can be correlated with respective maxima/minima in the reference oxygen isotopic curve, which correspond to almost all interglacial and glacial stages from MIS 19 to MIS 29 (Fig. 4). Note that a peak in the MDF_{ARM} parameter, which is not clearly expressed in the ARM_{20mT}/κ parameter, is used as a tie to MIS 21. This correlation implies only minor adjustments to a constant SAR model constrained by the M/B and UJ reversal boundaries alone. Constant SARs are assumed between tie points as shown by flat plateaus in the SAR plot of Fig. 5a. SAR values vary mostly from 2 to 3 cm/kyr, with somewhat lower values for the MIS 25/26 and MIS 23/24 glacial–interglacial transitions. In order to test this age model, both the age-tuned ARM_{20mT}/κ series for core LC07 and the oxygen isotope record for ODP Site 677 have been passed through a Gaussian filter centered on 20 kyr (0.05 kyr^{-1}), with a 0.02 kyr^{-1} bandwidth. The filter outputs (Fig. 5b) show fairly good agreement indicating that an accurate tuned solution has been

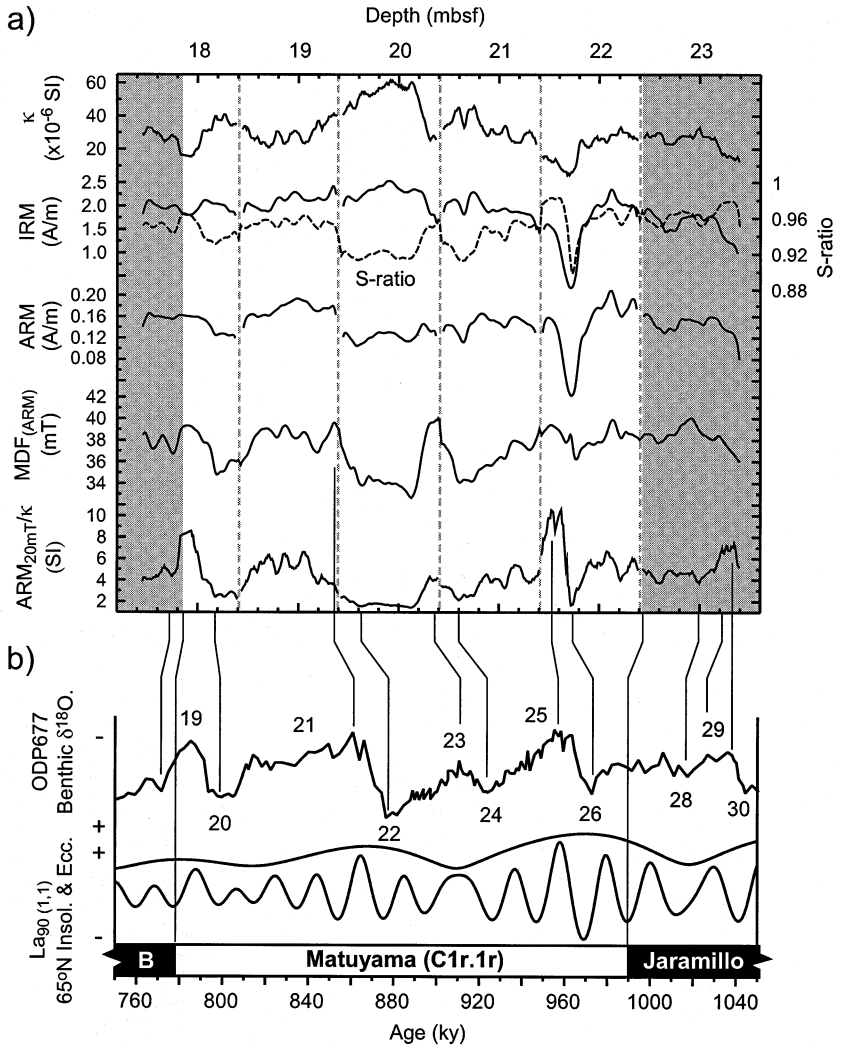

Fig. 4. (a) Down-core variations of the magnetic properties from 17.40 to 23.40 mbsf from core LC07: κ, low-field volume magnetic susceptibility; IRM; S-ratio; ARM; $MDF_{(ARM)}$, median destructive field of the ARM; ARM_{20mT}/κ ratio. Shaded areas denote the Brunhes Chron and the Jaramillo Subchron, respectively, and vertical dashed lines represent core breaks. (b) Astronomically tuned benthic $\delta^{18}O$ record for ODP Site 677 [21] with identification of isotopic stages; 65°N summer insolation and eccentricity curves of [43]. The tie points for deriving a detailed age model for core LC07 include the M/B and UJ reversals and prominent minima and maxima in rock magnetic parameters. The tie points are shown as correlation lines to maxima and minima in the isotopic curve (see text for discussion).

achieved. However, an additional peak is observed for core LC07 at around 810 kyr, corresponding to the younger part of the long interglacial MIS 21. We note that the isotopic record for ODP Site 677 is not well resolved at this interval and is dominated by relatively warm values in contrast with other records from the North Atlantic [27,28] where MIS 21 is interrupted by several cold periods. These fluctuations have been successfully correlated for ODP Site 983 [27] to the ice volume model derived from the 65°N summer insolation [29] (note that MIS 21 includes three insolation peaks, Fig. 4). Hence, we are satisfied with the presence of the extra peak in the

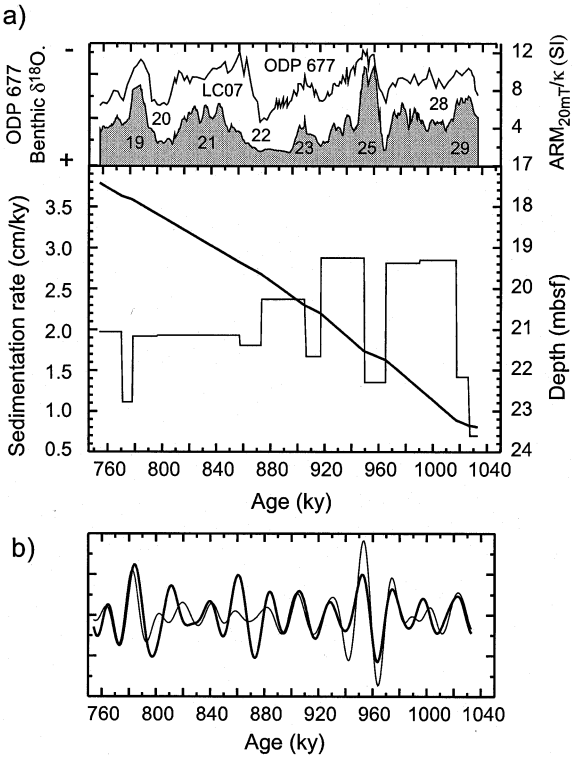

Fig. 5. (a) Benthic δ ^{18}O record for ODP Site 677 [21] and grain size parameter ARM_{20mT}/κ for site LC07 on a common age scale and age–depth map and interval sedimentation rates for the examined portion from core LC07. (b) Filter outputs (Gaussian filter centered on 20 kyr (0.05 kyr^{-1}) with a 0.02 kyr^{-1} bandpass) of the benthic δ ^{18}O record for ODP Site 677 (thick line) and the ARM_{20mT}/κ parameter for site LC07 (thin line).

filter output for core LC07 with respect to the one for ODP Site 677, and this is an additional argument in support of the accuracy of the achieved correlation. Moreover, coherence analysis of the spectra of the ODP Site 677 $\delta^{18}O$ data versus our two grain size proxies (MDF_{ARM} and ARM_{20mT}/κ) (Fig. 6) indicate significant coherence at most frequencies and comparable power at the climatic frequencies, which reinforces the validity of our age model.

Assuming the validity of the age model suggested above, and that magnetite dominates the ferrimagnetic fraction, it can be seen that warm interglacial periods are characterized by relatively small ferromagnetic grain (high ARM_{20mT}/κ ratios) (Fig. 4). Cold glacial events are dominated by the relatively coarser ferrimagnetic fraction (low ARM_{20mT}/κ values). Also, the relatively lower values of the *S*-ratio within the glacial periods (Fig. 4) indicate an increased high-coercivity contribution during glacial intervals. This may point toward an enhanced eolian input during the cold glacial periods.

3.4. Paleointensity determinations

The success of paleointensity determinations in sediments relies on using an appropriate NRM normalizing parameter in order to compensate for variations in concentration of ferrimagnetic grains. However, the choice of normalizer is not critical if the ChRM component has been properly isolated and the sediment is magnetically homogeneous [30]. It is clear, however, that the

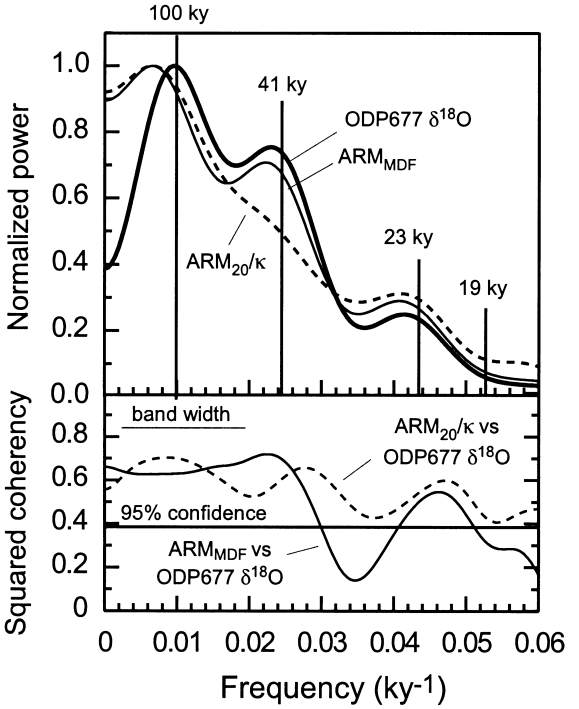

Fig. 6. Power spectra (Blackman–Tukey method with a Bartlett window) of $\delta^{18}O$ for ODP Site 677 (thick line), ARM_{MDF} (thin line) and ARM_{20mT}/κ (dashed line) in the studied interval of core LC07. The coherence between different parameters with the 95% confidence level (horizontal line) is plotted in the lower part of the figure.

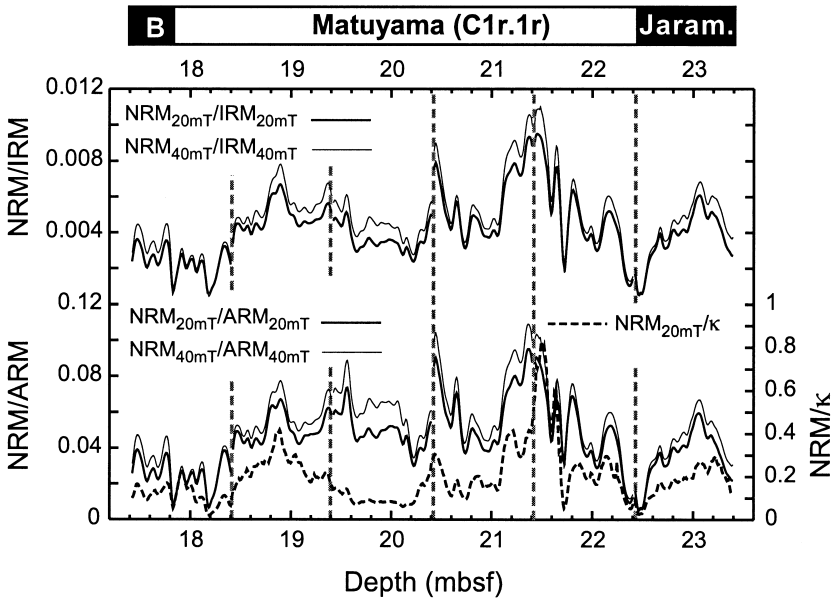

Fig. 7. Different normalized NRM curves (paleointensity proxies) for core LC07 (see text for discussion). Vertical shaded lines indicate core breaks.

chosen normalizing procedure has to activate the same relative spectrum of magnetic particles that is also responsible for the NRM [31]. The best normalizer is taken as the laboratory remanence (ARM, IRM) whose demagnetization curve (coercivity spectrum) most closely approximates that of the NRM. ARM normally activates the same magnetic grains as the most stable component of the NRM, whilst IRM is expected to activate larger magnetic grains in addition. Agreement between different normalization procedures is taken to indicate a successful paleointensity estimate.

In Fig. 7, relative paleointensity proxy records are plotted using different normalizers for the studied interval of core LC07. The NRM/ARM records after normalization at 20 mT and 40 mT demagnetization levels are comparable. This also applies to the IRM normalized intensity at the same demagnetization levels, which also show the same variability as the paleointensity derived using ARM as normalizer. The susceptibility-normalized curve shows a somewhat different variability, although common features with the other normalized records are evident. In Fig. 8, the coherence is shown between the three normalized

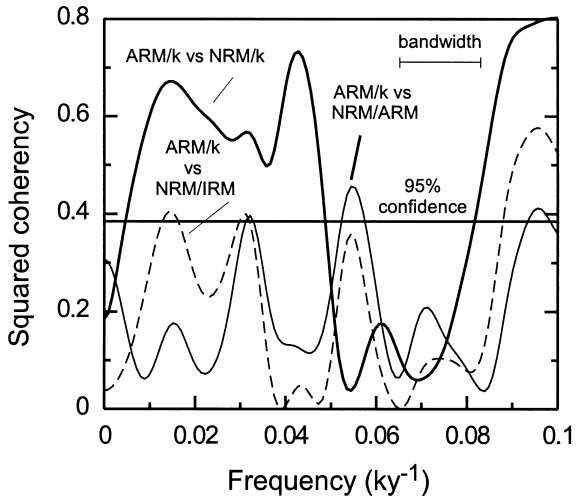

Fig. 8. Coherence functions of the ARM_{20mT}/κ ratio (climatic and grain size parameter) versus different NRM normalized values (paleointensity proxies). All NRM, ARM, and IRM intensities are after demagnetization at 20 mT. Coherence above the horizontal line is significant at a 95% confidence level. Only NRM/κ shows significant coherence over a wide range of frequencies and hence appears to be contaminated by climatic effects.

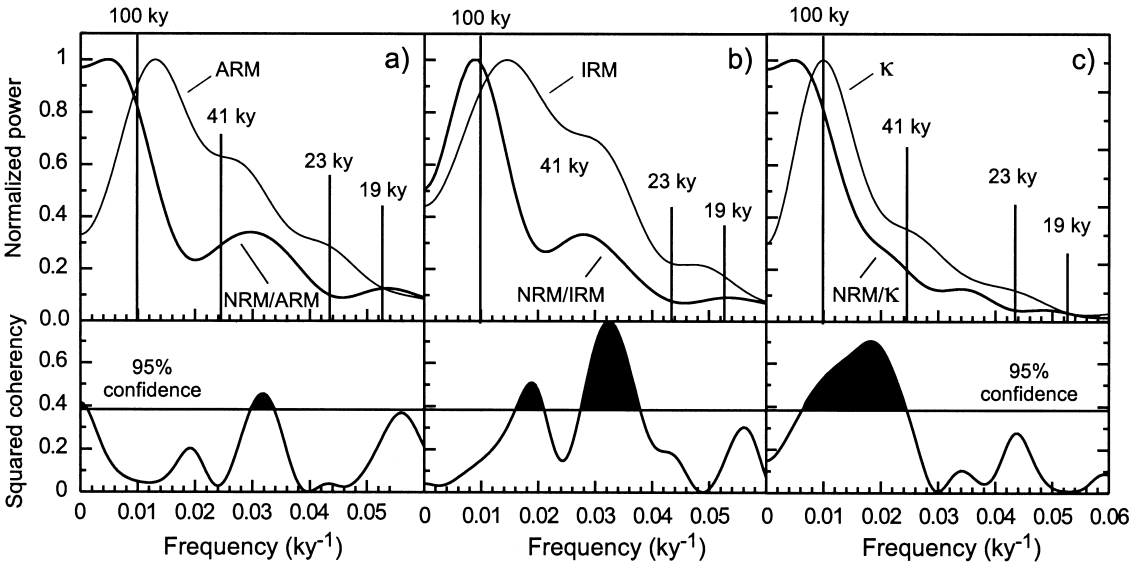

Fig. 9. Power spectra (Blackman–Tukey method with a Bartlett window) of (a) ARM, (b) IRM and (c) κ and normalized intensity using these parameters as normalizers in the studied interval of core LC07. The coherence between the normalized intensity and normalizing parameters is shown in the lower part of each diagram with coherence above the 95% confidence depicted in black.

paleointensity proxies with respect to the ARM_{20mT}/κ grain size parameter. As demonstrated in Fig. 5, ARM_{20mT}/κ in core LC07 is climatically controlled. The wide range of frequencies over which NRM/κ is coherent with ARM_{20mT}/κ indicates that κ normalization has not fully removed the lithological/climatic imprint in this case. Reduced coherence in the case of the ARM and IRM normalizers indicates that these parameters are more suitable for paleointensity normalization. In sedimentary paleointensity studies, the best normalizer is usually selected after coherence analysis between the candidate normalizers and the derived relative paleointensity [1] and it is suggested that coherence between the normalizer and paleointensity should not exceed the 95% confidence level. It has also been suggested [32] that further insights for selecting the optimal normalizer can be obtained from coherence analysis of the normalizer versus the NRM since a good normalizer will be highly correlated with the remanence. Coherence values for the three candidate normalizers and respective paleointensities in core LC07 are shown in Fig. 9.

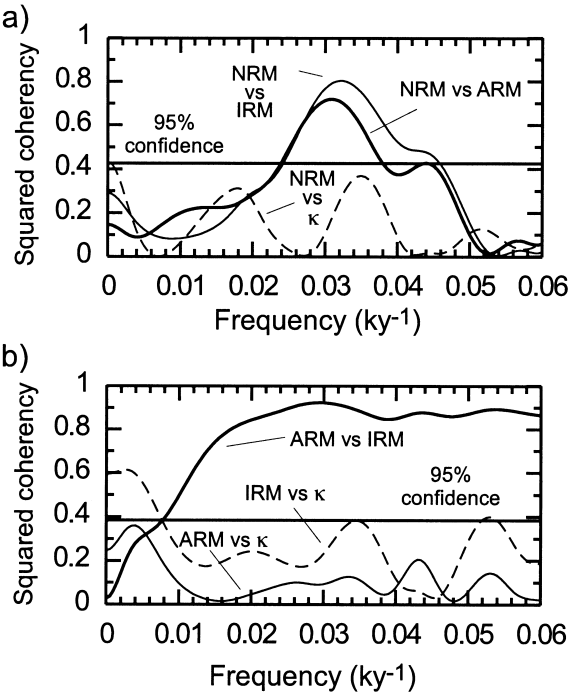

Fig. 10. (a) Coherence between NRM and candidate normalizers. (b) Coherence between the various candidate normalizers.

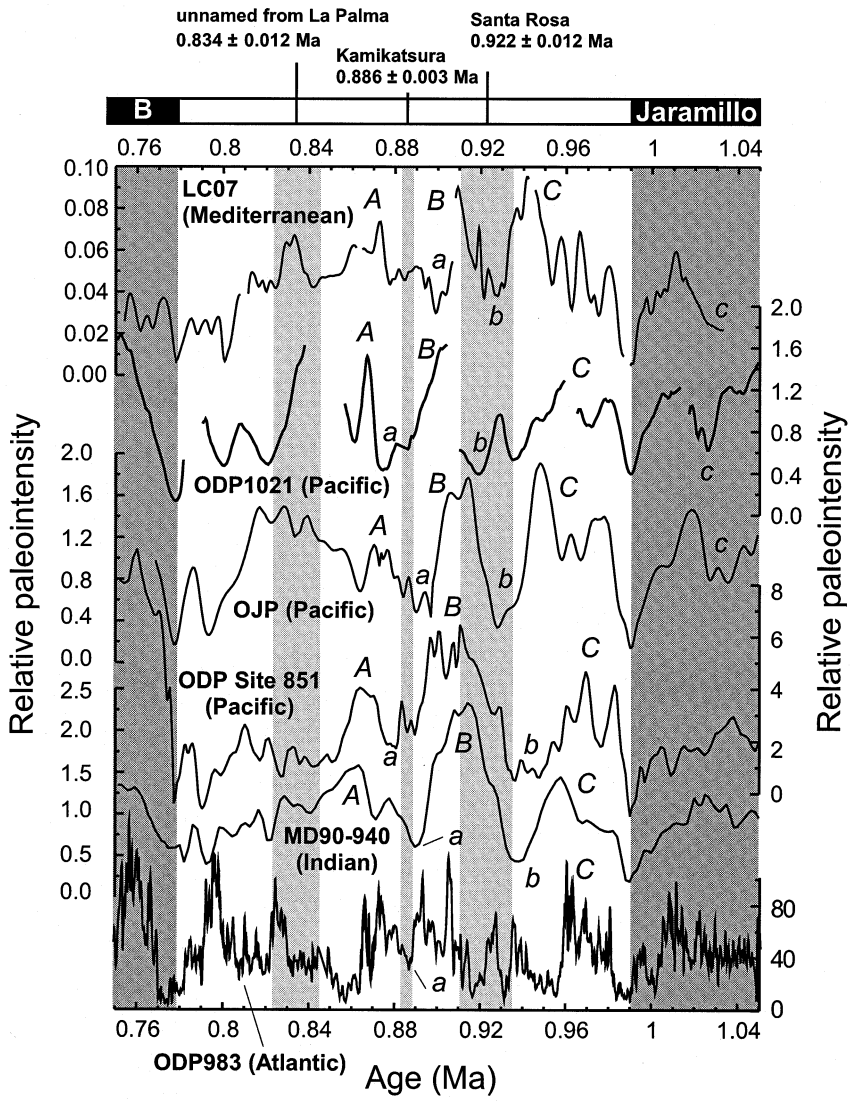

Fig. 11. Comparison of the paleointensity record obtained from core LC07 in this study with other published records from the Pacific (ODP Site 1021 [26], Ontong–Java Plateau stack (OJP) [8], and ODP Site 851 [6]), the Indian (MD90-940 [44]) and the Atlantic oceans (ODP Site 983 [28]). Published $^{40}Ar/^{39}Ar$ numerical ages of excursional lava units for the upper Matuyama Chron are indicated and represented as light shaded vertical strips, where the widths of the strips represent the respective error envelopes (Santa Rosa and Kamikatsura [34], unnamed from La Palma [35]).

Although the coherence for the three normalizers lies above the confidence level at certain frequencies, ARM appears to be the least coherent and therefore appears to be the best normalizer in core LC07. Coherence functions between NRM and the different normalizers for LC07 (Fig. 10a) indicate a lack of coherence for κ, whereas both ARM and IRM show significant coherence with NRM. Note also the high coherence between ARM and IRM (Fig. 4b). In summary, all approaches indicate that κ is not a suitable paleointensity normalizer in core LC07, whereas ARM and IRM are more suitable normalizers. The arithmetic mean of the NRM/ARM values at 20 mT and 40 mT is taken as the best paleointensity proxy for core LC07.

4. Discussion

The relative paleointensity record for core LC07 is plotted in Fig. 11 using the age model described above (754–1033 kyr) along with published records from the Pacific, Indian and Atlantic oceans. The M/B and UJ reversals occur within paleointensity minima in all the records. The astronomically calibrated ages of these reversals [19,20] allow us to put all the records onto a common time scale despite the fact that the type and accuracy of the detailed age models between those two tie points may differ among the records (see Table 1 for details of each record and tuning procedures). The paleointensity minimum $\sim$16 kyr before the M/B reversal is another common feature in all the examined records. Further common features in the examined paleointensity records are evident, but they either are not present in all the records, have a somewhat different expression (i.e., amplitude, power), or are slightly shifted in time among the records. Approximately equivalent features include relative paleointensity maxima at around 870 ka, 910 ka and 960 ka, which are labeled as *A*, *B* and *C*, respectively, in Fig. 11. Relative paleointensity minima occur between the *A*–*B* and *B*–*C* relative paleointensity maxima in all the records and are labeled *a* and *b*, respectively. A third conspicuous minimum (labeled *c*) is observed within the Jaramillo Subchron at $\sim$1.03 Ma in some of the records. The minima *a* and *b* have relative paleointensity values similar to or just higher than the paleointensity attained at the M/B and UJ reversals. Moreover, these two paleointensity minima are compatible with the age of $^{40}Ar/^{39}Ar$ dates from volcanic units from the Haleakala volcano, Hawaii, and Punuruu Valley, Tahiti [33], which contain transitional directions and may correspond to short polarity intervals or geomagnetic excursions (see below). A possible (unnamed) excursion, recorded in a lava flow with equatorial inclination and low paleointensity value from La Palma island, Spain, has been recently dated with the K/Ar method at 834 ± 12 ka [34]. This date and the associated excursion need to be validated, but it does not seem to have a clearly expressed paleointensity minimum in core LC07 and the other examined records (as would be expected for a geomagnetic excursion). Feature *a* in the paleointensity records corresponds well to the Kamikatsura event, while feature *b* matches the age of the Santa Rosa event in most of the records (Fig. 11) [33]. Differences in the exact position of the paleointensity features with respect to the age of the events from volcanic units may arise from inaccuracies or the particularities of the tuning method for a given sedimentary record (or lack of a robust age model). For instance, feature *b* has an older age in the ODP851 and MD90-940 records, while feature *a* appears to be slightly older in Mediterranean core LC07. It should be noted that the age model for core LC07 in the interval corresponding to glacial MIS 22 stage (Figs. 4 and 5) is constrained by a tie point corresponding to a minimum in the ARM_{20mT}/κ curve, and that positioning this point further down (older) in core LC07 would not violate the correlation and would bring event a to a slightly younger age in better agreement with the dating for the Kamikatsura event. Feature *c*,

Table 1
Sedimentary records used for comparison with LC07 in Fig. 11

Record	Lat N/Long E (°)	Water depth (m)	SAR (cm/kyr)	Dating	Normalization parameter	Reference
MD90-940	−06/061	3190	1	κ corr. with ODP 709	ARM (κ, IRM)	[44]
ODP851	02/250	3760	1.8	GRAPE astron. corr.	ARM (κ, IRM)	[6]
OJP	00/160	2806	1.2–1.8	magnetostratigraphy	thermal	[8]
LC07	38/010	488	2.3	RM astron. corr.	ARM (IRM)	this study
ODP1021	40/232	4213	$\sim$3	RM astron. corr.	κ (ARM)	[25]
ODP983	61/336	1983	$\sim$13	$\delta^{18}O$ astron. corr.	IRM (ARM)	[27]

GRAPE density, gamma ray attenuation porosity evaluation; RM, rock magnetic parameter; astron. corr., astronomical correlation.

which is located at the bottom of core LC07, is also present in the ODP 1021 and OJP records (Fig. 11). This feature has not yet been observed in volcanic rocks, but it might be associated with a geomagnetic excursion within the normal-polarity Jaramillo Subchron for which there is evidence in both marine and continental strata [35–39].

The presence of common features in all the sedimentary paleointensity records, together with the correspondence of the major paleointensity minima to full polarity reversals (M/B and UJ) and other numerically dated geomagnetic features recorded in volcanic rocks, validates the geomagnetic nature of the salient features from the sedimentary relative paleointensity records. Mediterranean core LC07 shares these features with the other examined records and therefore can be regarded as an appropriate core for geomagnetic studies.

Coherence between the ARM and the normalized paleointensity at some frequencies (Fig. 9a) suggests that the paleointensity record from core LC07 may not be fully free of lithological/climatic influences. Examining the coherence between the NRM/ARM the ARM_{20mT}/κ grain size ratio (Fig. 8) indicates slight significance at 0.054 kyr^{-1} (close to the 19 kyr precession peak at 0.0526 kyr^{-1}) which is an indication of possible climatic influence in the paleointensity proxy.

Evaluating the climatic imprint in any paleointensity record is complex because the same orbital parameters that force climate have been claimed to also drive the geodynamo [2,27]. The presence of power at some orbital frequencies in the paleointensity data, which were not obvious in the normalizer, has been taken to support the geomagnetic origin for the observed frequencies. This type of analysis on North Atlantic ODP Sites 983 and 984 cores led Channell and coworkers [2,27] to consider the significant power at the orbital obliquity frequency (centered on a period of $\sim$41 kyr) to be evidence for the orbital forcing of the geomagnetic field intensity (because power at this frequency in the IRM normalizer and bulk magnetic properties was not apparent in contrast to power at the $\sim$100 kyr eccentricity period which was inferred to contaminate the paleointensity record). However, a more sophisticated approach, using wavelet spectral analysis on the ODP Site 983 record covering the time interval 0–1.1 Ma [3], suggests that the orbital frequencies embedded in the paleointensity record are an expression of lithological variations and are probably not characteristic of the geodynamo. This illustrates the inherent complexities in the paleointensity data and the sensitiveness to the analytical procedure used to evaluate potential forcings in the geomagnetic field. Lack of a significant orbital obliquity component in the LC07 data therefore seems to validate the conclusion of Guyodo et al. [3] rather than earlier analyses, which suggest the orbital forcing of geomagnetic field intensity.

5. Conclusions

The rock magnetic properties from Mediterranean core LC07 indicate that magnetite is the dominant carrier of magnetic remanence. Stable magnetizations enable retrieval of a magnetostratigraphic record that spans the last $\sim$1.03 Ma and contains the M/B and UJ reversals. The duration of the M/B directional transition in core LC07 ($<$3000 years) is consistent with the estimation of $\sim$2300–5000 years from the compilation of Love and Mazaud [40], whose selection criteria considered 11 out of 62 studies of the M/B reversal. The estimate from core LC07 is also comparable with the inferred magnetic diffusion time ($\sim$3000 years) of the Earth's inner core which has been attributed as the mechanism that stabilizes the reversing field [41].

Variations of rock magnetic grain size parameters (e.g., ARM_{20mT}/κ) are climatically controlled and are used to derive a precise astronomically tuned age model for the interval between the M/B and UJ reversals by correlation to a target curve (the benthic $\delta^{18}O$ record from ODP Site 677 [20]). NRM/ARM is taken as the best paleointensity proxy in core LC07, although there may be some climatic influence embedded in the record. This is shown by spectral analysis of the 754–1033 kyr mean NRM/ARM record which shows significant power close to the 19 kyr precession periodicity. However, this overprint seems to be suf-

ficiently low that it does not obliterate the general character of the geomagnetic expression. Comparison of the paleointensity record from core LC07 with other published paleointensity records, tied together by pinning them at the astronomically tuned ages for the M/B and U/J reversals, reveals paleointensity minima that coincide with numerically dated volcanic units that record geomagnetic excursions (e.g., Santa Rosa at 0.92 Ma and Kamikatsura at 0.89 Ma).

Data from core LC07 (754–1033 ka) improve the restricted global paleointensity dataset for the late Matuyama Chron, which is essential for evaluating the long-term behavior of the geomagnetic field. The data from core LC07 are unprecedented from the Mediterranean basin where only a paleointensity record for the last 80 kyr was available to date [42].

Acknowledgements

This research was funded by EU Contract ERBFMRXCT98-0247. Y. Guyodo, J.E.T. Channell, Y. Kok and J.-P. Valet kindly provided data. We are grateful to two anonymous reviewers whose constructive comments helped to improve the manuscript. *[RV]*

References

[1] L. Tauxe, Sedimentary records of relative paleointensity of the geomagnetic field; theory and practice, Rev. Geophys. 31 (1993) 319–354.
[2] J.E.T. Channell, D.A. Hodell, J. McManus, B. Lehman, Orbital modulation of the Earth's magnetic field intensity, Nature 394 (1998) 464–468.
[3] Y. Guyodo, P. Gaillot, J.E.T. Channell, Wavelet analysis of relative geomagnetic paleointensity at ODP Site 983, Earth Planet. Sci. Lett. 184 (2000) 109–123.
[4] Y. Guyodo, J.-P. Valet, Relative variations in geomagnetic intensity from sedimentary records; the past 200,000 years, Earth Planet. Sci. Lett. 143 (1996) 23–36.
[5] Y. Guyodo, J.-P. Valet, Global changes in intensity of the Earth's magnetic field during the past 800 kyr, Nature 399 (1999) 249–252.
[6] J.-P. Valet, L. Meynadier, Geomagnetic field intensity and reversals during the past four million years, Nature 366 (1993) 234–238.
[7] Y.S. Kok, L. Tauxe, Saw-toothed pattern of sedimentary paleointensity records explained by cumulative viscous remanence, Earth Planet. Sci. Lett. 144 (1996) E9–E14.
[8] Y.S. Kok, L. Tauxe, A relative geomagnetic paleointensity stack from Ontong-Java Plateau sediments for the Matuyama, J. Geophys. Res. 104 (1999) 25,401–25,413.
[9] A.P. Roberts, J.S. Stoner, C. Richter, Coring-induced magnetic overprints and limitations of the long-core paleomagnetic measurement technique: some observations from Leg 160, eastern Mediterranean Sea, in: K.-C. Emeis, A.H.F. Robertson, C. Richter (Eds.), Proc. ODP, Init. Reports 160. Ocean Drilling Program, College Station, TX, 1996, pp. 497–505.
[10] B. Herr, M. Fuller, M. Haag, F. Heider, Influence of drilling on two records of the Matuyama/Brunhes polarity transition in marine sediment cores near Gran Canaria, in: P.P.E. Weaver, H.U. Schmincke, J.V. Firth (Eds.), Proc. ODP, Sci. Results 157. Ocean Drilling Program, College Station, TX, 1998, pp. 57–69.
[11] H. Vali, J.L. Kirschvink, Magnetofossil dissolution in a paleomagnetically unstable deep-sea sediment, Nature 339 (1989) 203–206.
[12] J.A. Tarduno, Temporal trends of magnetic dissolution in the pelagic realm gauging paleoproductivity?, Earth Planet. Sci. Lett. 123 (1994) 39–48.
[13] M. Torii, Low-temperature oxidation and subsequent downcore dissolution of magnetite in deep-sea sediments, ODP Leg 161 (Western Mediterranean), J. Geomagn. Geoelectr. 49 (1997) 1233–1245.
[14] J.E.T. Channell, T. Hawthorne, Progressive dissolution of titanomagnetites at ODP Site 653 (Tyrrhenian Sea), Earth Planet. Sci. Lett. 96 (1990) 469–480.
[15] A.P. Roberts, J.S. Stoner, C. Richter, Diagenetic magnetic enhancement of sapropels from the eastern Mediterranean Sea, Mar. Geol. 153 (1999) 103–116.
[16] L. Tauxe, J.L. LaBrecque, R. Dodson, M. Fuller, U-channels – a new technique for paleomagnetic analysis of hydraulic piston cores, EOS Trans. AGU 64 (1983) 219.
[17] R. Weeks, C. Laj, L. Endignoux, M. Fuller, A. Roberts, R. Manganne, E. Blanchard, W. Goree, Improvements in long-core measurement techniques; applications in palaeomagnetism and palaeoceanography, Geophys. J. Int. 114 (1993) 651–662.
[18] J.L. Kirschvink, The least-squares line and plane and the analysis of palaeomagnetic data, Geophys. J. R. Astron. Soc. 62 (1980) 699–718.
[19] L. Tauxe, T. Herbert, N.J. Shackleton, Y.S. Kok, Astronomical calibration of the Matuyama-Brunhes boundary: Consequences for magnetic remanence acquisition in marine carbonates and the Asian loess sequences, Earth Planet. Sci. Lett. 140 (1996) 133–146.
[20] N. Shackleton, A. Berger, W.R. Peltier, An alternative astronomical calibration of the lower Pleistocene timescale based on ODP Site 677, Trans. R. Soc. Edinburgh Earth Sci. 81 (1990) 251–261.

[21] D.V. Kent, D.A. Schneider, Correlation of paleointensity variation records in the Brunhes/Matuyama polarity transition interval, Earth Planet. Sci. Lett. 129 (1995) 135–144.
[22] P. Hartl, L. Tauxe, A precursor to the Matuyama/Brunhes transition-field instability as recorded in pelagic sediments, Earth Planet. Sci. Lett. 138 (1996) 121–135.
[23] J.W. King, S.K. Banerjee, J.A. Marvin, Ö. Özdemir, A comparison of different magnetic methods for determining the relative grain size of magnetite in natural materials some results from lake sediments, Earth Planet. Sci. Lett. 59 (1982) 404–419.
[24] S.G. Robinson, The late Pleistocene paleoclimatic record of North Atlantic deep-sea sediments revealed by mineral-magnetic measurements, Phys. Earth. Planet. Inter. 42 (1986) 22–47.
[25] Y. Guyodo, C. Richter, J.-P. Valet, Paleointensity record from Pleistocene sediments (1.4–0 Ma) off the California Margin, J. Geophys. Res. 104 (1999) 22,953–22,964.
[26] D. Paillard, L. Labeyrie, P. Yiou, Macintosh program performs time-series analysis, EOS Trans. AGU 77 (1996) 339.
[27] J.E.T. Channell, H.F. Kleiven, Geomagnetic palaeointensities and astrochronological ages for the Matuyama-Brunhes boundary and the boundaries of the Jaramillo subchron; palaeomagnetic and oxygen isotope records from ODP Site 983, Phil. Trans. R. Soc. London 358 (2000) 1027–1047.
[28] R. Tiedemann, M. Sarnthein, N.J. Shackleton, Astronomic timescale for the Pliocene Atlantic $\delta^{18}O$ and dust flux records of Ocean Drilling Program Site 659, Paleoceanography 9 (1994) 619–638.
[29] J. Imbrie, J.Z. Imbrie, Modeling the climatic response to orbital variations, Science 207 (1980) 943–953.
[30] J.-P. Valet, L. Meynadier, A comparison of different techniques for relative paleointensity, Geophys. Res. Lett. 25 (1998) 89–92.
[31] S. Levi, S.K. Banerjee, On the possibility of obtaining relative paleointensities from lake sediments, Earth Planet. Sci. Lett. 29 (1976) 219–226.
[32] C. Constable, L. Tauxe, R.L. Parker, Analysis of 11 Myr of geomagnetic intensity variation, J. Geophys. Res. 103 (1998) 17735–17748.
[33] B.S. Singer, K.A. Hoffman, A. Chauvin, R.S. Coe, M.S. Pringle, Dating transitionally magnetized lavas of the late Matuyama Chron; toward a new $^{40}Ar/^{39}Ar$ timescale of reversals and events, J. Geophys. Res. 104 (1999) 679–693.
[34] X. Quidelleur, P. Gillot, Evidence for a new geomagnetic excursion recorded prior to the M.B transition at La Palma, EOS Trans. AGU 81 (48, Fall Meet. Suppl.), Abstract V72E-09, 2000.
[35] B.J. Pillans, A.P. Roberts, G.S. Wilson, S.T. Abbott, B.V. Alloway, Magnetostratigraphic, lithostratigraphic and tephrostratigraphic constraints on lower and middle Pleistocene sea-level changes, Wanganui Basin, New Zealand, Earth Planet. Sci. Lett. 121 (1994) 81–98.
[36] R.-X. Zhu, C. Laj, A. Mazaud, The Matuyama-Brunhes and Upper Jaramillo transitions recorded in a loess section at Weinan, north-central China, Earth Planet. Sci. Lett. 125 (1994) 143–158.
[37] G. McIntosh, T.C. Rolph, J. Shaw, P. Dagley, A detailed record of normal-reversed-polarity transition obtained from a thick loess sequence at Jiuzhoutai, near Lanzhou, China, Geophys. J. Int. 127 (1996) 651–664.
[38] C. Richter, A.P. Roberts, J.S. Stoner, L.D. Benning, C.T. Chi, Magnetostratigraphy of Pliocene–Pleistocene sediments from the eastern Mediterranean Sea, in: A.H.F. Robertson, K.C. Emeis, C. Richter (Eds.), Proc. ODP, Sci. Results 160. Ocean Drilling Program, College Station, TX, 1998, pp. 61–73.
[39] D.K. Biswas, M. Hyodo, Y. Taniguchi, M. Kaneko, S. Katoh, H. Sato, Y. Kinugasa, K. Mizuno, Magnetostratigraphy of Plio-Pleistocene sediments in a 1700-m core from Osaka Bay, southwestern Japan and short geomagnetic events in the middle Matuyama and early Brunhes chrons, Palaeogeogr. Palaeoclimatol. Palaeoecol. 148 (1999) 233–248.
[40] J.J. Love, A. Mazaud, A database for the Matuyama-Brunhes magnetic reversal, Phys. Earth Planet. Inter. 103 (1997) 207–245.
[41] D. Gubbins, The distinction between geomagnetic excursions and reversals, Geophys. J. Int. 137 (1999) F1–F3.
[42] E. Tric, J.P. Valet, P. Tucholka, M. Paterne, L.D. Labeyrie, F. Guichard, L. Tauxe, M. Fontugne, Paleointensity of the geomagnetic field during the last 80,000 years, J. Geophys. Res. 97 (1992) 9337–9351.
[43] J. Laskar, The chaotic motion of the solar system a numerical estimate of the size of the chaotic zones, Icarus 88 (1990) 266–291.
[44] L. Meynadier, J.-P. Valet, F.C. Bassinot, N.J. Shackleton, Y. Guyodo, Asymmetrical saw-tooth pattern of the geomagnetic field intensity from equatorial sediments in the Pacific and Indian oceans, Earth Planet. Sci. Lett. 126 (1994) 109–127.